

Structural and optical characterizations of Ni (II) tetraphenyl porphyrin thin films

M.M. El-Nahass^{1,a}, H.M. Abd El-Khalek², and A.M. Nawar²

¹ Physics Department, Faculty of Education, Ain Shams University, Heliopolis, Roxy, Cairo, Egypt

² Thin Film Laboratory, Physics Department, Faculty of Science, Suez Canal University, Ismailia, Egypt

Received: 16 July 2011 / Received in final form: 14 December 2011 / Accepted: 31 January 2012
Published online: 1 March 2012 – © EDP Sciences 2012

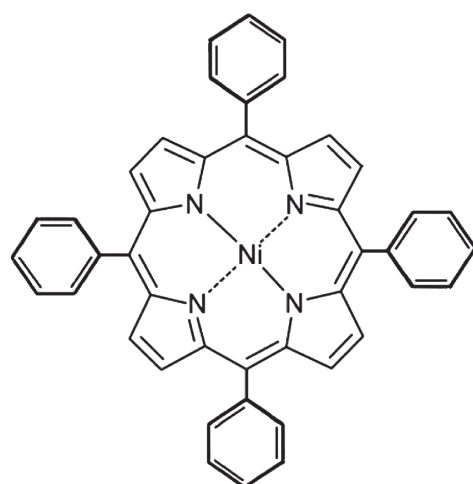
Abstract. Thermal evaporation technique was used to prepare thin films of 5,10,15,20-tetraphenyl-21H,23H-porphine nickel (II), NiTPP, onto glass and quartz substrates. The crystal structures and morphologies of all prepared NiTPP thin films were investigated at 298, 423 and 573 K by using X-ray diffraction, XRD, and scan electron microscopy, SEM, respectively. The lattice of all prepared NiTPP films was investigated as a monoclinic with space group P2/M. The surface topography of the prepared films showed granular particles of sizes 49.7, 64.7 and 107 nm. The annealed NiTPP films at 423 K have a spatial configuration of well-defined grains boundary with nanoporous nature and all annealed films at 573 K have higher aggregates and the porosity of the films was increased. Optical constants namely refractive index, n , and the absorption index, k , of NiTPP films have been estimated by using spectrophotometric measurements of transmittance and reflectance in the spectral range from 200 to 2500 nm. The absorption spectra in the UV-vis spectrum were analyzed in terms of both molecular orbital and band theories. The obtained data of n and k were used to estimate the type of transitions and were found to be indirect transition for all films. The optical and fundamental gaps were decreased as the annealing temperature was increased. Some optical parameters namely molar extinction coefficient, ϵ_{molar} , oscillator strength, f , and electric dipole strength, q^2 , have been evaluated. According to the single oscillator model and Drude model, some related parameters such as oscillation energy, E_o , the dispersion energy, E_d , the optical dielectric constant, ϵ_∞ , the lattice dielectric constant, ϵ_L , and the ratio of free carrier concentration to its effective mass, N/m^* , the third-order nonlinear susceptibility, $\chi^{(3)}$, and molar polarizability, α_p , were estimated before and after annealing.

1 Introduction

Porphyrins are a class of conjugated macrocyclic compounds in which four pyrrole rings are linked to each other in cyclic fashion through *meso*-carbon bridges. Photoprocesses in porphyrins, metalloporphyrins and related compounds have captured considerable attention not only because of their important place in nature, but also because these molecules offer promise as components of artificial solar energy capture and storage devices, elements in molecular logic circuits and chromophores in drugs for photodynamic therapy [1–5]. In order to exploit the properties of porphyrins, they can be deposited as thin films by using several techniques such as solvent casting, Langmuir-Blodgett [6,7], spin coating, high vacuum evaporation [8,9] and glow discharge induced sublimation [10]. The difference in properties like the geometric, electronic structure, optical and vibrational spectra of porphyrin may be related to the nature of metal atom at the center of the porphyrin molecule and the introduction of

substituent in meso position [11]. One interesting property of the tetrapyrrole derivatives is their great third-order optical nonlinearity attributed to their highly polarizable extended two-dimensional π electron system [12,13]. Porphyrin thin films have been attracting interest as an organic material for optoelectronic devices such as optical data recording media by means of photochemical hole burning of metal-free base porphyrins [14]. An important fact emphasizes the significance of thin film spectroscopy in application to condensed molecular matter. The point is that due to the weak Van der Waals interaction between the molecules in the films, their optical properties are not significantly changed when compared with the free molecule [15]. Porphyrins present optical absorption and fluorescence bands in the visible region related to the electronic transitions of the aromatic systems. The interactions of analytes with porphyrin thin films affect both the optically active transitions of the single molecule and the π - π interactions between macrocycles, giving rise to detectable changes of the optical absorption spectra. This property allowed developing several opto-chemical sensing

^a e-mail: prof_nahhas@yahoo.com



5, 10, 15, 20 -Tetraphenyl-21H, 23H-porphine nickel (II)

Product Number	252204
Product Brand	ALDRICH
CAS Number	14172-92-0
MDL number	MFCD00010727
Pub. Chem. Substance ID	24855191
TEST	SPECIFICATION
Appearance (Color)	Purple to Dark Purple
Appearance (Form)	Solid Crystalline Powder
Purity (HPLC)	≥ 95.0 %
Wavelength	409 - 415 nm
Extinction Coefficient	≥200000
Carbon	≥ 74.8 %
Nitrogen	≥ 7.9 %
Linear Formula	C ₄₄ H ₂₈ N ₄ Ni
Molecular Weight	671.41

Fig. 1. (Color online) The molecular structure and details of the NiTPP compound.

procedures [16,17]. The high π electron density, resulting in an extended electron delocalization, makes porphyrins useful for observing a variety of nonlinear optical effects. Their sharp absorption bands in the visible and NIR can be used for resonance enhancement of $\chi^{(3)}$ [18]. As well, they have enormous potential for applications on the technological front, which include optical limiting [19,20] and optical switching [21]. They have also been used as organic semiconductor [22] and bistable devices [23,24]. Despite the existence of a few reports in the literature studying some physical properties of Ni (II) tetraphenyl porphyrin, NiTPP thin films [25–27], much of the optical properties of NiTPP are unknown. The lack of data in the literature concerning the optical characterization of NiTPP films confirms the significance of this investigation. Also, to the best of our knowledge there is no thorough study of its optical properties, as reported here. Therefore, the objective of this study is to investigate the structural and optical properties of thermally evaporated thin films including the refractive index, n , and the extinction coefficient, k , over the spectral range 200–2500 nm, and examine the effect of annealing temperatures on their structural, morphological and optical properties.

2 Experimental procedures

A dark purple crystalline powder 5,10,15,20-tetraphenyl-21H,23H-porphine nickel (II), NiTPP, was purchased from Aldrich Chem. Co. and was used as-received without further purification. The schematic diagram of the NiTPP molecular structure is shown in Figure 1. Using Edward E306A, England coating unit, thin films were prepared by thermal evaporation under vacuum of 2×10^{-4} Pa on ten glass substrates for structure exploration, and five fused

optically flat quartz substrates for optical measurements. The glass and quartz substrates were carefully cleaned by putting them in chromic acid for 15 min and then they were washed several times with distilled water. After that, the substrates were rinsed by isopropyl alcohol. The substrates were dried in a steam of dry nitrogen and finally were cleaned by atomic bombardment in an initial stage of evacuation. Evaporation of the material was carried out with a quartz crucible heated by a tungsten coil. The substrates were maintained at room temperature during deposition. The evaporation rates as well as the film thickness of the evaporated films were controlled by using a quartz crystal monitor Edward FTM6 model, the deposition rate was controlled at 2 nm/s. After the preparation of NiTPP thin films, the films were divided into five groups; each group contains a NiTPP film on glass substrate and the other on quartz substrate. The first group remained as-deposited at 298 K. The groups from the second to the fifth were annealed, respectively, at 423, 473, 523 and 573 K under roughing vacuum at 10^{-1} Pa with a soaking time of 1 h. Film thicknesses were also subsequently calibrated interferometrically by Tolansky's method [28].

The crystal structure of 5,10,15,20-tetraphenyl-21H, 23H-porphine nickel (II), NiTPP, for powder and thin films was investigated by X-ray diffraction patterns. X-ray diffractometer, Philips model X'pert, with utilized monochromatic Cu-K α radiation of $\lambda = 1.54056$ Å and was operated at 40 kV and 25 mA. The diffraction patterns were recorded automatically with a scanning speed of $2^\circ/\text{min}$. Scanning electron microscope Philips XL30 was used to investigate the structural features of the surface morphologies of the NiTPP thin films.

A computer-aided double-beam spectrophotometer (JASCO model V-570 UV-vis-NIR) was used to measure

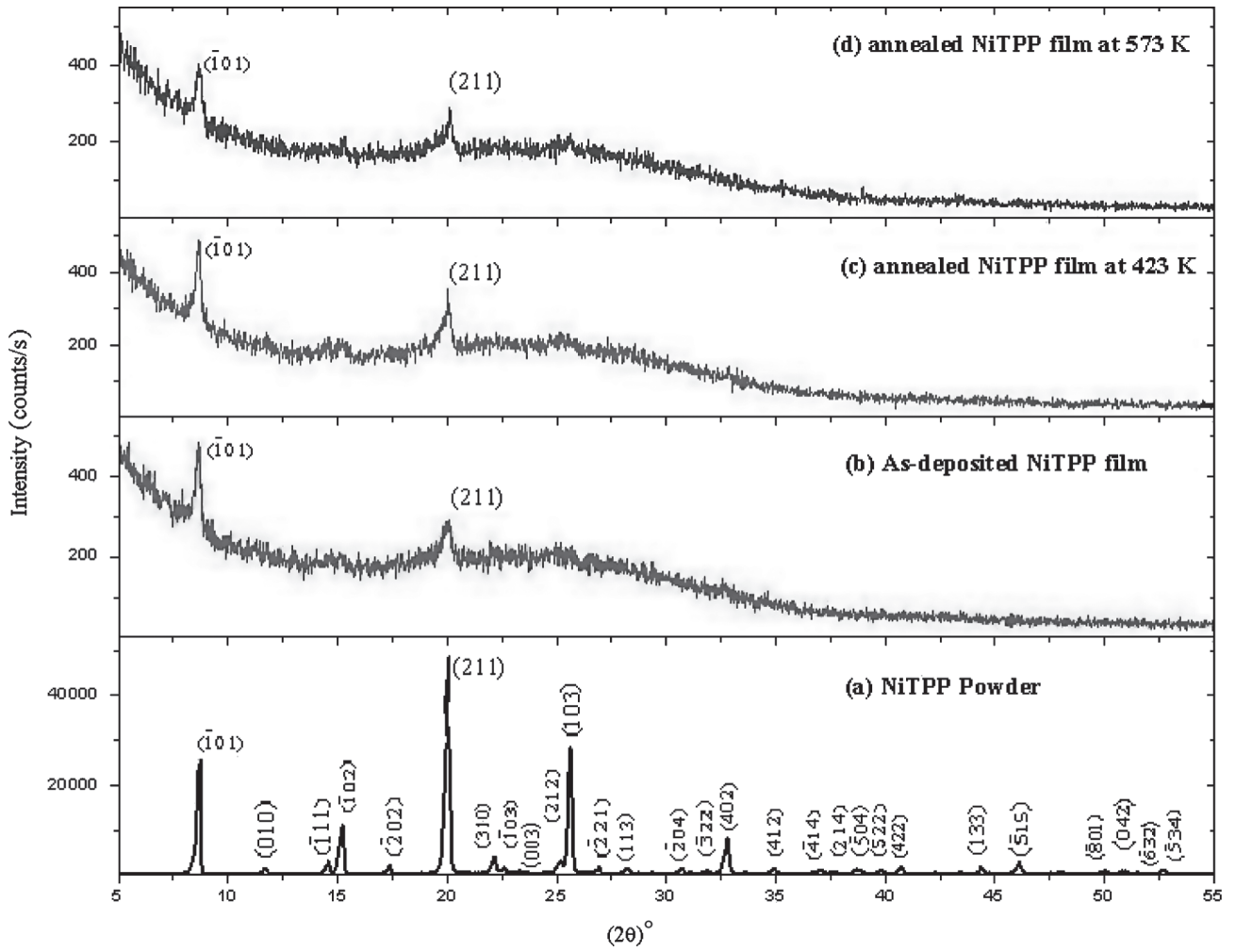


Fig. 2. (Color online) X-ray diffraction patterns of NiTPP in the form of: (a) powder, (b) as-deposited film, (c) annealed film at 423 K and (d) annealed film at 573 K.

the transmittance $T(\lambda)$ at the normal incidence of the light in the spectral range 200–2500 nm; the spectrophotometer is also provided with a constant angle 5° specular reflection attachment to measure the reflectance, $R(\lambda)$, in the same spectral range. A blank quartz identical substrate to the one used for the thin film deposition was used as a reference for the transmission scan. However, the reflection scan was taken using Al mirror as a reference in the same measured range of the wavelength. The relative uncertainty for $T(\lambda)$ and $R(\lambda)$ measurements given by the manufacturer is $\pm 1\%$. All structural and optical measurements have been performed on the samples at room temperature 298 K.

3 Determination of optical constants

The spectral data obtained directly from the spectrophotometer were transformed to absolute values after corrections of the absorbance and reflectance of the substrate.

The absolute values of T and R are given by [29]:

$$T = \left(\frac{I_{ft}}{I_q} \right) (1 - R_q), \quad (1)$$

where R_q is the reflectance of quartz substrate and I_{ft} , I_q are the intensities of light passing through quartz system and reference quartz substrate, respectively.

$$R = \left(\frac{I_{fr}}{I_m} \right) R_m [(1 - R_q)^2 + 1] - T^2 R_q, \quad (2)$$

where I_m is the intensity of light reflected from the reference mirror, I_{fr} is the intensity of light reflected from the sample reaching the detector and R_m is the mirror reflectance.

In order to calculate the optical constants, the absorption coefficient, α , the absorption index, k , and the refractive index, n , of the films at different wavelengths, we can

use the following equations [30]:

$$\alpha = \left(\frac{1}{d}\right) \ln \left[\frac{(1-R)^2}{2T} + \sqrt{\frac{(1-R)^4}{4T^2} + R^2} \right], \quad (3a)$$

$$k = \frac{\alpha\lambda}{4\pi}, \quad (3b)$$

$$n = \frac{1+R}{1-R} + \sqrt{\frac{4R}{(1-R)^2} - k^2}, \quad (4)$$

where α is the absorption coefficient and d is the film thickness. The experimental error in measuring the film thickness was taken as $\pm 2\%$, in T and R as $\pm 1\%$ and in the calculated values of (n) and (k) as $\pm 3\%$ and $\pm 2.5\%$, respectively.

4 Results and discussion

4.1 X-ray diffraction analysis

X-ray powder diffraction, XRD, of 5,10,15,20-tetraphenyl-21H,23H-porphine nickel (II), NiTPP, was taken for the first time in a 2θ range from 5° to 55° , and its spectrum is presented in Figure 2a. The pattern has many diffraction peaks with different intensities indicating that the powder of NiTPP has a polycrystalline nature. The highest preferred orientation is found along the $(2\ 1\ 1)$ plane. The unit cell parameters of NiTPP were determined for the first time by using the CRYSFIRE computer program [31]. Therefore, the deduced indexing can be accepted and the NiTPP lattice as monoclinic with space group P2/M. The lattice parameters; $a = 14.622\ \text{\AA}$, $b = 7.566\ \text{\AA}$, $c = 11.785\ \text{\AA}$ and $\beta = 104.11^\circ$. Table 1 shows the values of Miller indices, $(h\ k\ l)$, for each diffraction peak together with the interplanar spacing, (d_{hkl}) , obtained by using CHECKCELL program [32]. Our check cell is in agreement with [33–36], but it is in disagreement with reference [37], this is may be because the authors have not defined the purity of extracted Ni-porphyrin. Also, the data of check cell for NiTPP films of thickness 138 nm are in disagreement with reference [38]. May be, because the structure was considered as a rare example for a planar nickel (II) porphyrin, as *meso*-substituted nickel (II) porphyrins with either only *meso*-aryl or with *meso*-alkyl residues typically exhibit a ruffled conformation [38]. The patterns of diffractograms (b)–(d) in Figure 2 indicate that as-deposited and annealed NiTPP films are partially crystallized with a preferential orientation in the $(\bar{1}\ 0\ 1)$ and $(2\ 1\ 1)$ direction. Results also show that annealing temperatures increases the degree of crystallinity of NiTPP films.

4.2 Surface topology analysis

The surface topography and grain shape growth for as-deposited and annealed NiTPP thin films are investigated

Table 1. The diffraction spacings, d_{measured} , the Miller indices $(h\ k\ l)$, and the relative intensity, I/I_0 , for NiTPP in the powder form.

No.	$2\theta_{\text{measured}}$	d_{measured}	$d_{\text{calculated}}$	I/I_0	$(h\ k\ l)$
1	8.69054	10.16649	10.196	74.3	$(\bar{1}\ 0\ 1)$
2	11.68328	7.56814	7.566	2.53	$(0\ 1\ 0)$
3	14.85524	6.06821	6.076	5.84	$(\bar{1}\ 1\ 1)$
4	15.24562	5.80682	5.815	21.69	$(\bar{1}\ 0\ 2)$
5	17.38391	5.09707	5.098	4.11	$(\bar{2}\ 0\ 2)$
6	20.05887	4.42298	4.427	100	$(2\ 1\ 1)$
7	22.1505	4.00983	4.009	8.34	$(3\ 1\ 0)$
8	22.62015	3.92762	3.927	2.95	$(\bar{1}\ 0\ 3)$
9	23.32318	3.8108	3.81	1.21	$(0\ 0\ 3)$
10	25.18634	3.53296	3.535	6.23	$(2\ 1\ 2)$
11	25.63499	3.47213	3.473	58.61	$(1\ 0\ 3)$
12	26.94198	3.30659	3.308	3.17	$(2\ 2\ 1)$
13	28.20449	3.16138	3.157	2.94	$(1\ 1\ 3)$
14	30.73265	2.90683	2.907	2.24	$(\bar{2}\ 0\ 4)$
15	31.87918	2.80486	2.804	1.73	$(\bar{3}\ 2\ 2)$
16	32.78117	2.72971	2.729	16.83	$(4\ 0\ 2)$
17	34.92044	2.56723	2.567	2.81	$(4\ 1\ 2)$
18	37.10033	2.42124	2.416	171	$(\bar{4}\ 1\ 4)$
19	38.56727	2.33245	2.332	1.28	$(2\ 1\ 4)$
20	38.86828	2.31508	2.315	1.37	$(\bar{5}\ 0\ 4)$
21	39.72460	2.26712	2.266	1.59	$(\bar{5}\ 2\ 2)$
22	40.75012	2.21241	2.213	2.71	$(4\ 2\ 2)$
23	44.34830	2.04089	2.041	2.96	$(1\ 3\ 3)$
24	46.09813	1.96741	1.969	5.23	$(\bar{5}\ 1\ 5)$
25	50.01447	1.82214	1.82	1.81	$(\bar{8}\ 0\ 1)$
26	50.78751	1.79621	1.796	1.36	$(0\ 4\ 2)$
27	52.59174	1.73876	1.739	1.71	$(\bar{6}\ 3\ 2)$
28	52.71000	1.73513	1.705	1.73	$(\bar{5}\ 3\ 4)$

by scanning electron microscopy, SEM, as shown in Figure 3. The topograph (a) in Figure 3 depicts that the particles have granular shape of sizes 49.7, 64.7 and 107 nm, some porous regions on the film surface and also in between the grains [39]. The topograph (b) in Figure 3 depicts the surface microstructure properties of the annealed NiTPP film at 423 K, with nanoporous nature and a spatial configuration of well-defined grain boundary [39,40]. The topograph (c) in Figure 3 depicts the influence of annealing temperature at 573 K, higher aggregates and more pores appear rather than those appearing in an as-deposited film. We conclude that the crystal growth of the particles is affected by the annealing temperatures and this behavior can play roles in the film topographies. In other words, the thermal annealing can modify the surface topographies of NiTPP films by controlling the aggregate densification and porous properties of NiTPP [40]; in turn, these effects may be used in controlling the optical properties of NiTPP thin films.

4.3 Optical properties

4.3.1 Transmission and reflection spectra

Figure 4 illustrates the spectral behaviors of transmittance, $T(\lambda)$, and reflectance, $R(\lambda)$, in the wavelength range

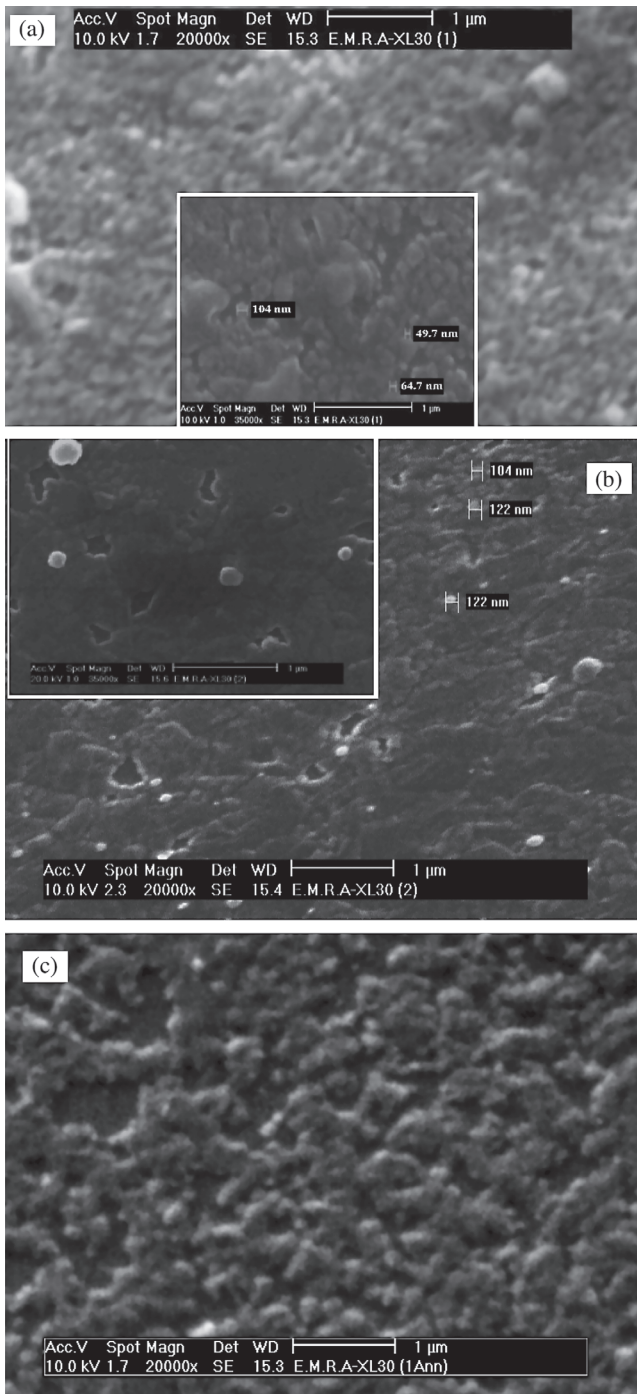


Fig. 3. The SEM micrographs for (a) as-deposited, (b) annealed film at 423 K and (c) annealed film at 573 K NiTPP thin film.

200–2500 nm for as-deposited and annealed NiTPP thin films of thickness 138 nm. The spectra can be divided into two regions: (I) in the wavelength range 200–1000 nm, the total sum of $T(\lambda)$ and $R(\lambda)$ is less than unity, absorption region, implies the absorption existence and (II) at longer wavelength, $\lambda > 1000$ nm, the film becomes transparent and no light is scattered or absorbed, $T + R \approx 1$, in the non-absorbing region. It can be observed that the behavior

of T and R in the transparent region is the same for all films before and after annealing; this indicated that all films have almost the same thickness and are within the experimental errors $\pm 2\%$. The transmittance edge shifts toward longer wavelengths as a result of annealing temperatures.

4.3.2 Refractive index spectra

Figure 5 shows the behavior of real part, n , of the refractive index for as-deposited and annealed NiTPP thin films. The inset in Figure 5 depicts that the refractive index for as-deposited and annealed films exhibits an anomalous dispersion in the range $\lambda < 1000$ nm, which can be explained according to the multi-oscillator model [41]. The refractive index for all films exhibits a normal dispersion in the range $\lambda > 1000$ nm, which can be understood by using the single oscillator model [42,43]. The results for the real part, n , show three peaks at 210, 300 and 390 nm in the UV range and one peak in the blue region at 480 nm. The intensities of these peaks are descending, i.e., decrease with increasing the annealing temperature. Also, there are two peaks in the yellow region at 540 and 570 nm; the results reveal that the positions of the estimated peaks are stable under the influence of annealing temperatures. The effect of annealing temperatures on NiTPP thin films is in good agreement with the results in reference [44].

4.3.3 Absorption characterizations

The absorption coefficient, α , of as-deposited and annealed NiTPP thin films is calculated by using the absolute values of transmittance, $T(\lambda)$, and the reflectance, $R(\lambda)$. Figure 6 depicts the variation of absorption coefficient, α , with the wavelengths for as-deposited and annealed NiTPP films in UV-vis spectrum. The conjugated tetraphenyl porphyrin macrocycle with central nickel atom shows high intense absorption termed Soret band, which appears in the wavelength range 330–490 nm [45]. The interaction between two or more molecules in the unit cell of the aggregate results in two or more excitonic transitions with high transition moment and the original absorption band (the Soret band has two peaks, B_X and B_Y at 383 nm and 443 nm, respectively) splits into two or more by splitting, maybe due to vibronic coupling in the excited state Davydov splitting [46]. The absorption peaks and shoulder in the wavelength region 500–640 nm are named Q -band and extend with longer wavelengths in red and IR region with lower absorption. The other three closed bands labeled (N, M and L) appear in the UV region. The peaks of Q and B bands are assigned π - π^* transition between bonding and anti-bonding molecular orbitals [47]. The two interband transitions Q and B are from the two highest occupied molecular orbital (HOMO) levels $1a_{1u}(\pi)$ and $4a_{2u}(\pi)$ to the first excited lowest unoccupied molecular orbital (LUMO) level $5e_g(\pi^*)$ [48,49]. The influence of annealing temperatures on absorption spectra appears with,

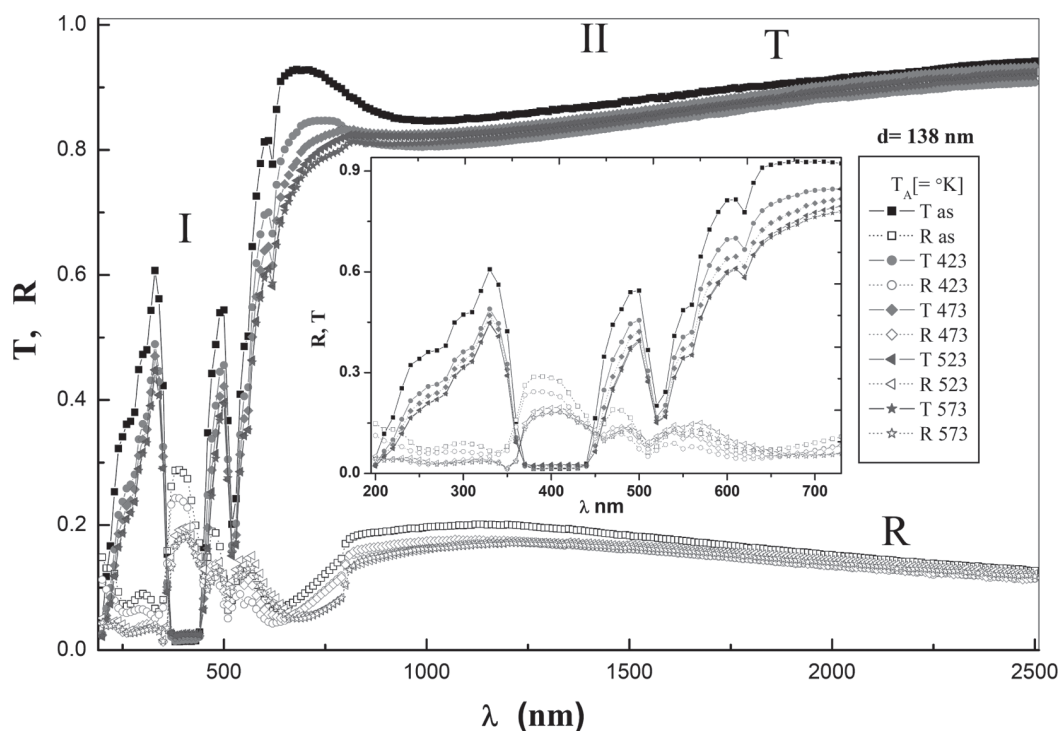


Fig. 4. (Color online) Transmittance $T(\lambda)$, and reflectance, $R(\lambda)$, spectra for as-deposited and annealed NiTPP thin films.

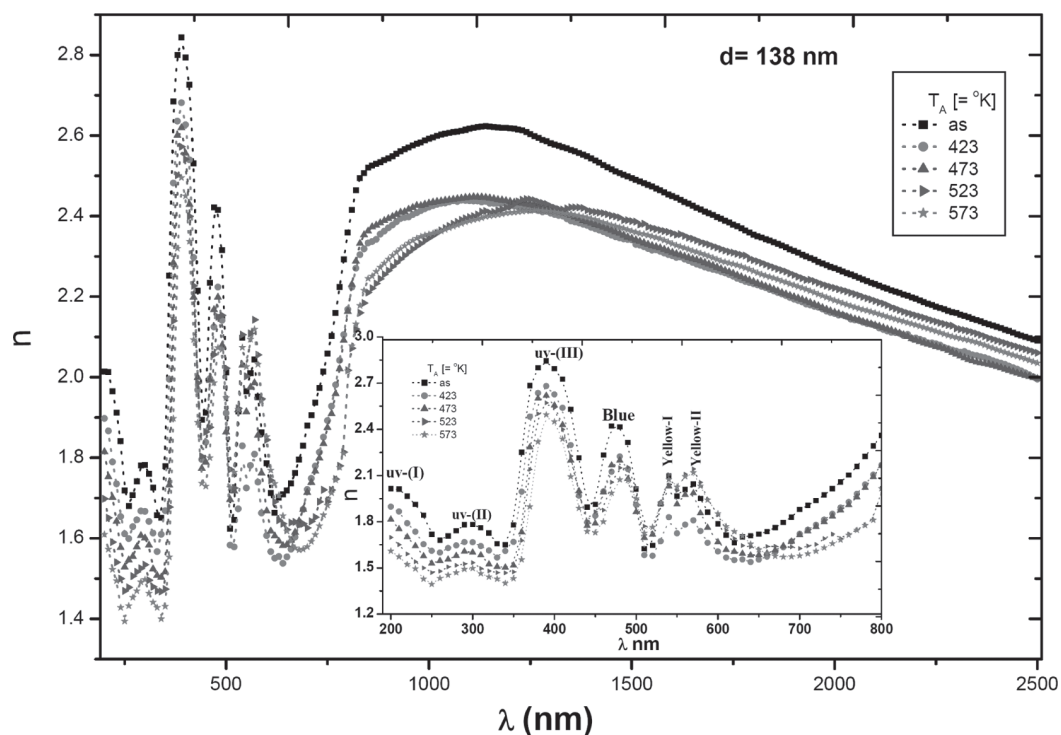


Fig. 5. (Color online) The dispersion curve of refractive index, $n(\lambda)$, for the as-deposited and annealed NiTPP thin films, the inset figure shows the dependence of the anomalous spectrum on the annealing temperature for as-deposited and annealed NiTPP thin films.

slight, changes in significant broadening in the Soret band and red shift of Q -bands. These changes indicate an increase in π -conjugations due to the increase in NiTPP planarity [50,51].

Intensities of the absorption bands are evaluated by calculating their oscillator strength, f , which is usually proportional to the area under the absorption line shapes. The oscillator strength, f , the electric dipole strength, q^2 ,

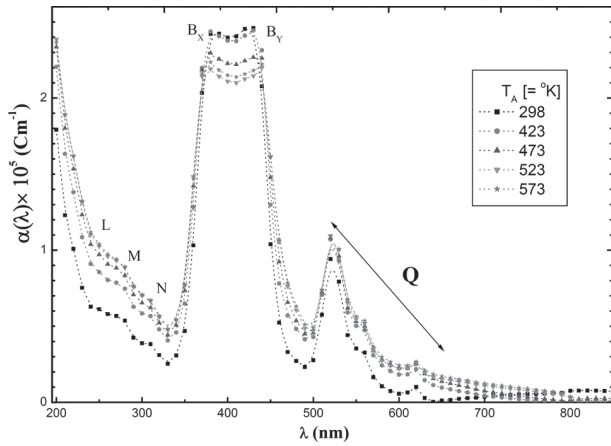


Fig. 6. (Color online) The optical absorption coefficient, $\alpha(\lambda)$, versus wavelength, λ , for as-deposited and annealed NiTPP thin films.

and the absorption half-band width, $\Delta\lambda$, for the as-deposited and annealed NiTPP thin films can be estimated by relating the absorption coefficient, α , to the molar extinction coefficient, $\varepsilon_{\text{molar}}$, which is often used to describe the absorption of light by nonsolid molecular media by using the expressions [52,53]:

$$\alpha(h\nu) = \left(\frac{\rho_m}{M_w} \right) \times 10^3 \ln(10) \varepsilon_{\text{molar}} = \text{const.} \cdot \varepsilon_{\text{molar}}, \quad (5)$$

$$f = 4.3 \int \varepsilon_{\text{molar}}(\nu) d\nu, \quad (6)$$

$$q^2 = \left(\frac{1}{2500} \right) \varepsilon_{\text{molar}} \left[\frac{\Delta\lambda}{\lambda} \right], \quad (7)$$

where M_w is the molecular weight of NiTPP, ρ_m is the density of mass and $\varepsilon_{\text{molar}}(\nu)$ is the molar extinction coefficient which is corresponding to the transition frequency, ν (cm^{-1}). Figure 7 shows the plot of $\varepsilon_{\text{molar}}$ as a function of wavenumber, (ν) , for as-deposited and annealed NiTPP thin films. The calculated values of the oscillator strength and the electric dipole strength for as-deposited and annealed NiTPP films are listed in Table 2.

For a crystalline and amorphous semiconducting material, the analysis of optical absorption near the absorption band edge is a standard method for determining the types of transitions and calculation of the optical band gap. The energy dependence of the interband absorption coefficient for direct and indirect allowed transitions is given by the following expression [54].

For allowed direct transitions:

$$\alpha(h\nu) = B_d (h\nu - E_g^d)^{1/2}. \quad (8a)$$

For indirect allowed transitions:

$$\alpha(h\nu) = B_{\text{ind}} (h\nu - E_g^{\text{ind}} \pm E_{\text{ph}})^2. \quad (8b)$$

In the above equations, E_g^d and E_g^{ind} represent the band gap energies, B_d and B_{ind} are characteristic constant

parameters, independent of photon energy, for direct and indirect transitions, respectively, and E_{ph} is the phonon energy associated to indirect transition. The graph of $(\alpha h\nu)^2$ versus $(h\nu)$ is found not to support the interpretation of direct rather than indirect band gap. Figure 8 shows the $(\alpha h\nu)^{1/2}$ versus $(h\nu)$ plots for as-deposited and annealed NiTPP films. The values of indirect optical band gaps for the as-deposited and annealed NiTPP films are evaluated from the x -axis intercepts at $(\alpha h\nu)^{1/2} = 0$. It should also be noted that, the optical gap, E_g^{onset} , corresponds to the onset of optical absorption and formation of a bound electron-hole pair, or exciton ‘‘Frenkel exciton’’ [55], but the fundamental energy gap, E_g , is the energy gap between valence band ‘‘ π -band’’ and conduction band ‘‘ π^* -band’’ [56]. Figure 9 depicts the variation of E_g^{onset} and E_g with annealing temperatures, the annealing temperature has a significant effect on them; as the temperature increases from 298 to 573 K, the E_g shows a substantial decrease from 2.58 to 2.39 eV, while E_g^{onset} decreases from 1.92 to 1.15 eV. The decrease in the E_g^{onset} and E_g , because of the thermal annealing, results in more delocalized π -electrons, the lowering of the band gap between π and π^* , and the increase of the optical (π - π^*)-transition which results in the observed red shift in the gap [57]. The values of optical gap, E_g^{onset} , and the fundamental energy gap, E_g , for NiTPP, FeTPPCl [44] and CoMTPP [48] are listed in Table 3.

4.3.4 Dispersion parameters

The observed dispersion behavior can be explained if it is assumed to be the response of a set of Lorentzian oscillators of adjustable strength and position [58]. Using the previous postulation, the refractive index as a function of photon energy can be analyzed on the basis of the single oscillator model, for photon energies below the interband absorption edge. Wemple and DiDomenico researched dispersion data for more than 100 different materials, both covalent and ionic and both crystalline and amorphous, and they introduced two important parameters: one is named, E_d , to describe the dispersion energy of the refractive index and the second named single oscillator energy, E_o . Using these parameters, the refractive index can be expressed as [42,43]:

$$(n^2 - 1)^{-1} = \frac{E_o}{E_d} + \frac{1}{E_o E_d} (h\nu)^2. \quad (9)$$

The relation between $(n^2 - 1)^{-1}$ versus $(h\nu)^2$ for as-deposited and annealed NiTPP films is illustrated in Figure 10. E_o and E_d are directly determined from the slope, $(E_o/E_d)^{-1}$, and the intersection, (E_o/E_d) , with the vertical axis. The calculated values of the dispersion parameters (E_o and E_d), as well as the corresponding high frequency optical dielectric constant ($\varepsilon_\infty = n^2$) for as-deposited and annealed NiTPP films, are listed in Table 4.

The refractive index data are analyzed to obtain the lattice dielectric constant for examining the contribution

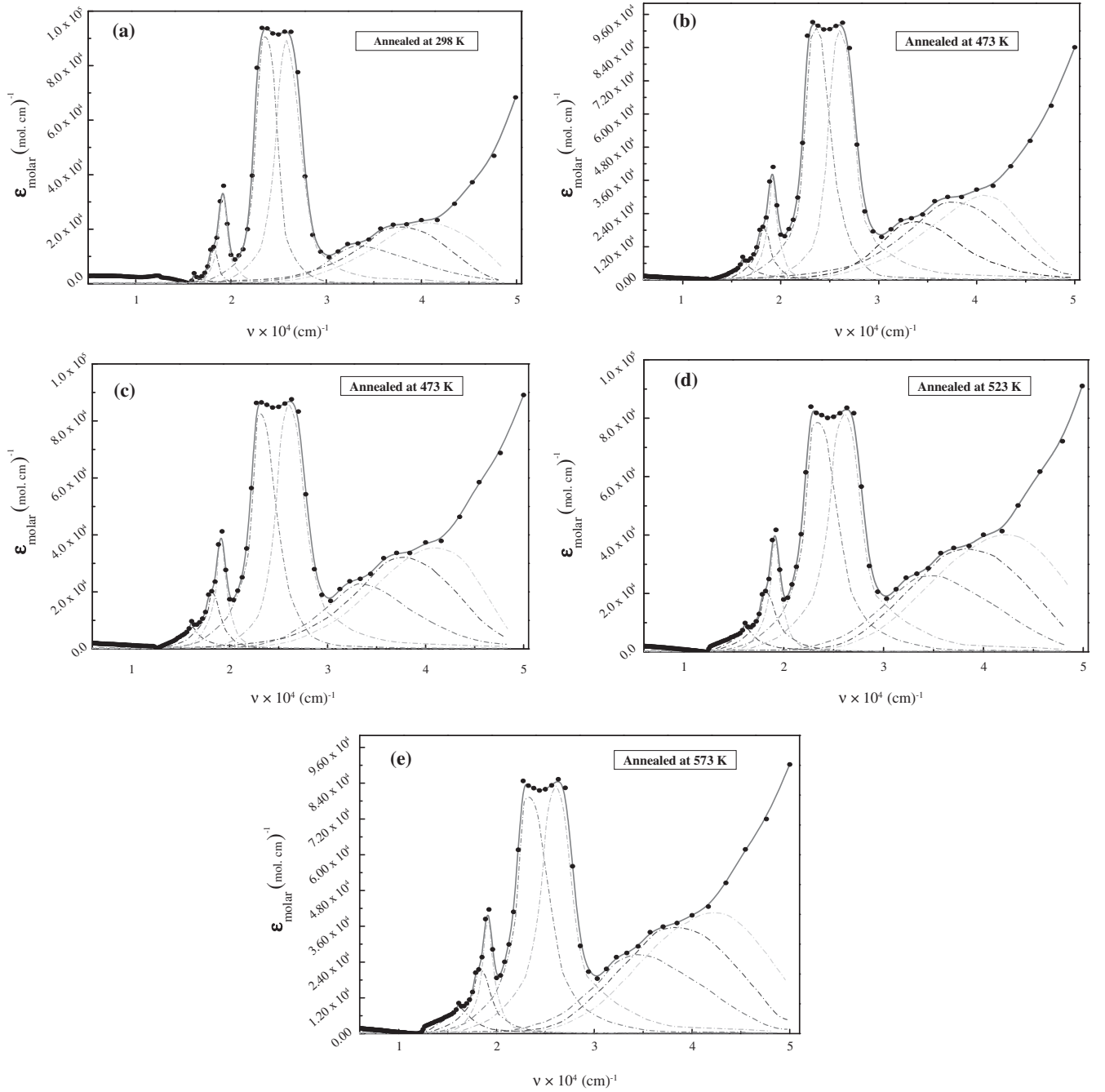


Fig. 7. (Color online) Figure (a)–(e) shows the plot of ϵ_{molar} as a function of the frequency, ν , for as-deposited and annealed NiTPP thin films.

of the free carriers and also to indicate the lattice vibration modes of the dispersion. The dependence of the refractive index on the wavelength can be expressed as follows [56, 59, 60]:

$$\epsilon_1 = n^2 = \epsilon_L - \left(\frac{e^2}{4\pi^2 c^2 \epsilon_o} \right) \left(\frac{N}{m^*} \right) \lambda^2, \quad (10)$$

where ϵ_1 is the real part of dielectric constant, ϵ_L is the lattice dielectric constant, e is the elementary charge, ϵ_o is the permittivity of free space, c is the speed of light

and N/m^* is the ratio of free carrier concentration to its effective mass. Figure 11 shows the relation between n^2 and λ^2 for as-deposited and annealed NiTPP films. It is observed that the dependence of n^2 on λ^2 is linear at longer wavelengths, where extrapolating linear part to zero wavelengths gives the value of ϵ_L , whereas N/m^* value is estimated from the slope. The estimated value of ϵ_L and ϵ_∞ for as-deposited and annealed NiTPP films is listed in Table 4. The value of difference between ϵ_∞ and ϵ_L is decreased with increasing the influence of annealing;

Table 2. The values of the absorption half-band width, $\Delta\lambda$, the maximum wavelength, λ_{\max} , the oscillator strength, f , and electric dipole strength, q^2 , for the as-deposited and the annealed NiTPP thin films.

T (K)	Oscillator name	λ_{\max} (nm)	$\Delta\lambda$ (nm)	f	q^2 (\AA^2)	Oscillator name	λ_{\max} (nm)	$\Delta\lambda$ (nm)	f	q^2 (\AA^2)
298	Osc 1	164	12	0.015	0.07	Osc 5	259	25	1.22	3.5
423		164	21	0.062	0.28		261	26	1.27	3.62
473		162	22	0.078	0.35		262	27	1.31	3.71
523		162	25	0.097	0.44		261	32	1.39	3.95
573		161	28	0.124	0.56		261	31	1.39	3.95
298	Osc 2	182	9	0.064	0.26	Osc 6	348	93	0.64	1.38
423		182	16	0.149	0.6		343	86	0.93	2.02
473		182	20	0.183	0.74		341	94	1.09	2.38
523		183	23	0.225	0.91		355	11	1.53	3.2
573		184	23	0.244	0.98		355	11	1.54	3.22
298	Osc 3	191	10	0.164	0.63	Osc 7	378	95	1.05	2.25
423		191	12	0.198	0.77		343	86	0.93	2.02
473		191	13	0.226	0.88		378	103	1.76	3.46
523		191	13	0.226	0.87		385	115	2.2	4.29
573		191	13	0.236	0.92		386	116	2.25	4.33
298	Osc 4	237	21	1.1	3.47	Osc 8	404	106	1.28	2.36
423		237	27	1.3	4.09		398	100	1.6	3
473		234	26	1.2	3.66		401	105	2	3.77
523		237	33	1.4	4.46		416	130	2.8	5.05
573		237	33	1.4	4.47		416	130	2.84	5.07

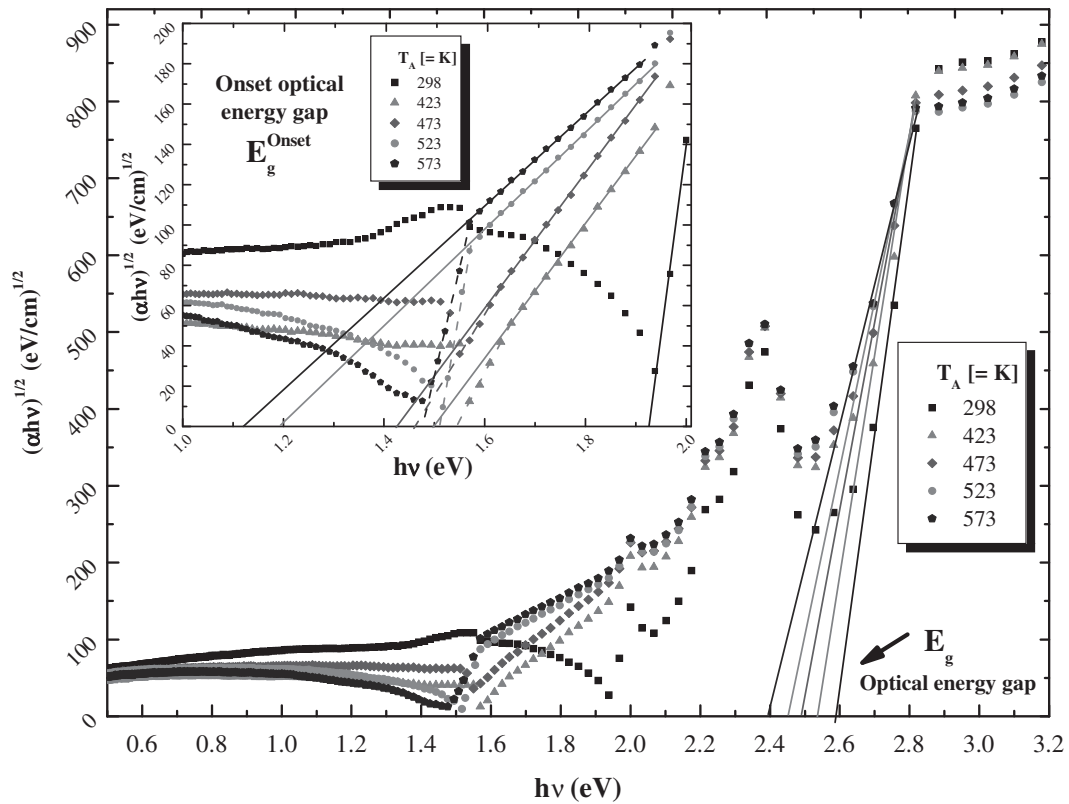
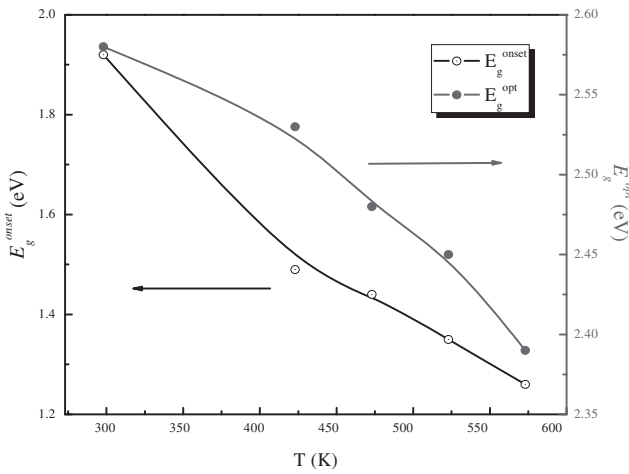
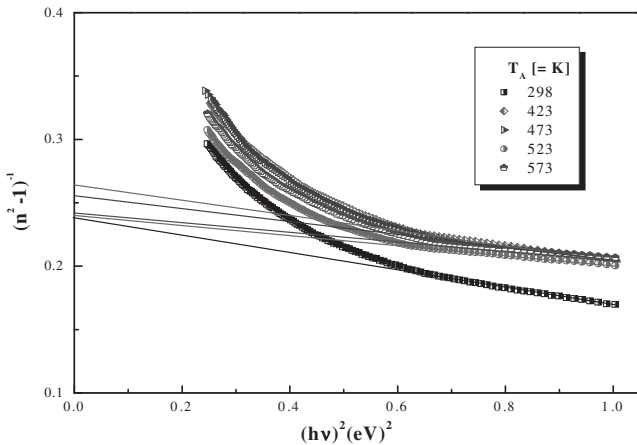


Fig. 8. (Color online) The relation between $(\alpha h\nu)^{1/2}$ and photon energy, $h\nu$, for as-deposited and annealed NiTPP thin films.

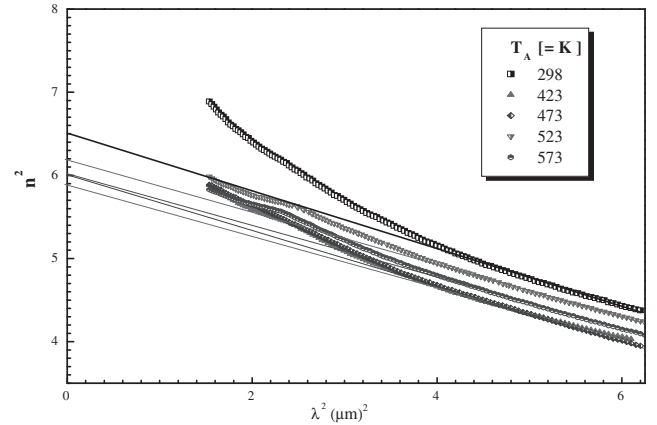
Table 3. The optical parameters of indirect transitions for the as-deposited and the annealed NiTTP, FeTPPCL and CoMTPP thin films.

Film condition	Influence of annealing temperatures						Heat treatment			
	NiTTP			FeTPPCL [44]			CoMTPP [48]			
	T (K)	E_g^{onset} (eV)	E_{ph} (meV)	E_g (eV)	T (K)	E_g^{onset} (eV)	E_g (eV)	T (K)	E_g^{onset} (eV)	E_g (eV)
As-deposited	298	1.92	–	2.58	298	1.63	2.49	298	1.58	3
Annealed	423	1.49	47	2.53	423	1.61	2.42	–	–	–
	473	1.44	34.6	2.48	473	1.56	2.24	–	–	–
	523	1.19	317	2.45	523	1.51	2	–	–	–
	573	1.15	283	2.39	–	–	–	573	1.16	2.83


Fig. 9. (Color online) Variation of the energy gaps E_g^{onset} and E_g^{opt} as a function of annealing temperatures for as-deposited and annealed NiTTP thin films.

Fig. 10. (Color online) The plots of $(n^2 - 1)^{-1}$ versus $(h\nu)^2$ for as-deposited and annealed NiTTP thin films.

this means that the lattice vibration and bounded carriers in an empty lattice in the transparent region decrease with the increase of the annealing influence [61, 62].

One interesting property of the tetrapyrrole derivatives is their great third-order optical nonlinearity attributed to their highly polarizable extended two-dimensional


Fig. 11. (Color online) The plots of n^2 versus λ^2 for as-deposited and annealed NiTTP thin films.

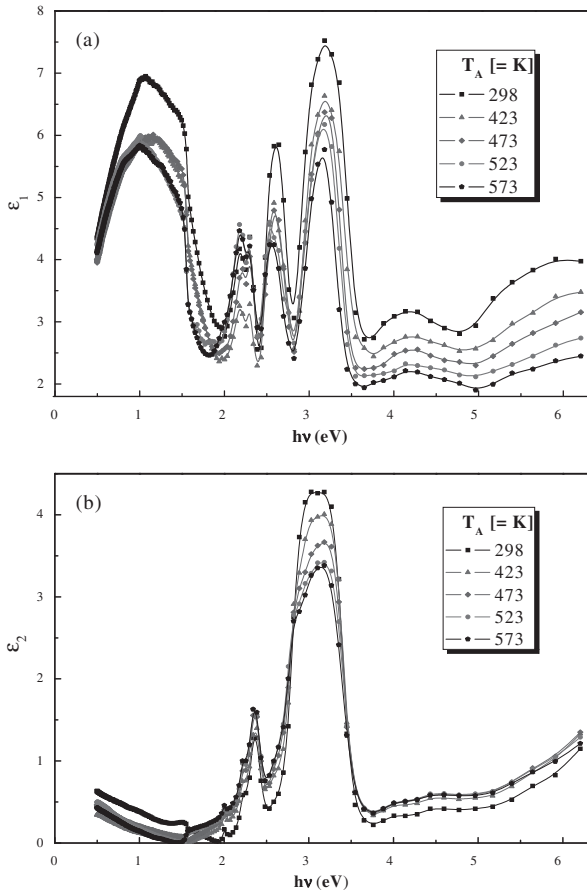
π -electron system. According to Miller's generalized rule [63, 64], the estimated values of the third-order nonlinear optical susceptibility, $\chi^{(3)}$, for the as-deposited and annealed NiTTP films are calculated and recorded in Table 4 from the following equation [42, 43, 56, 65]:

$$\chi^{(3)} = \frac{A}{(4\pi)^4} [n_o^2 - 1]^4, \quad (11)$$

where A is a quantity that is assumed to be frequency independent and nearly the same for all materials, $A \approx 1.7 \times 10^{-10}$ esu [63, 64], and the third-order nonlinear optical susceptibility, $\chi^{(3)}$, in the limit $h\nu \rightarrow 0$ ($n = n_o$). The different processes for determining the value of third-order nonlinear optical susceptibility are anticipated to be a base for the production of all high-frequency ultrafast optical switches and photonic devices [66]. According to the thermal stability of NiTTP [67], the estimated peaks for as-deposited and annealed NiTTP thin films are 1.08, 2.58 and 3.18 eV which show an optical switching behavior [68]. Where the third-order nonlinear optical susceptibility reaches its maximum value at the first estimated peak 1.08 eV and decreases to its minimum value when the photon energy is equal to the value of the onset optical absorption energy for as-deposited and annealed NiTTP films.

Table 4. The dispersion parameters of the as-deposited and the annealed NiTTP thin films.

Film condition	T (K)	E_o (eV)	E_d (eV)	ε_∞	ε_L	N/m^* ($\text{kg}^{-1} \text{m}^{-3}$)	$\chi^{(3)} \times 10^{-12}$ (esu)	α_p (\AA^3)
As-deposited	298	1.85	7.7	5.2	6.5	4.6×10^{56}	2.05	88
Annealed	423	2.12	8	4.85	5.87	4.8×10^{56}	1.38	85
	473	2.3	9.1	4.91	6.03	4.2×10^{56}	1.66	85.6
	523	2.45	10.2	5.12	6.2	3.9×10^{56}	2.04	87.5
	573	2.6	10.6	5.04	6.06	4.0×10^{56}	1.87	86.8


Fig. 12. (Color online) The plots of (a) the real dielectric constant, ε_1 , and (b) the imaginary dielectric constant, ε_2 , versus photon energy, $h\nu$, for the as-deposited and annealed NiTTP films.

4.3.5 Dielectric constant

The complex dielectric, $\tilde{\varepsilon}$, constant is an important quantity for the design of highly efficient optoelectronic devices, because the dielectric constant gives amenable characterizing view about the interactions between photons and electrons in a material. These interactions can be observed on the shapes of the real, ε_1 , and imaginary, ε_2 , parts of the dielectric constant in the dielectric spectrum [69–71]. The complex dielectric constant is described by:

$$\tilde{\varepsilon}(h\nu) = \varepsilon_1(h\nu) + i\varepsilon_2(h\nu), \quad (12)$$

where $\varepsilon_1 (= n^2 - k^2)$ is the real part and $\varepsilon_2 (= 2nk)$ is the imaginary part of the dielectric constant. Figure 12a and b shows the spectra of real and imaginary parts which are called dispersion and absorption curves, respectively. The behavior of ε_1 follows the same trend as (n), whereas the behavior of ε_2 mainly follows the behavior of (k) which is related to the variation of with photon energy.

The molar refractivity, α_p (molar polarizability), of NiTTP films can be deduced according to Clausius-Mossotti's equation [72–75]:

$$\alpha_p = \left(\frac{\varepsilon_\infty - 1}{\varepsilon_\infty + 2} \right) \left[\frac{3M_w}{4\pi\rho_m N_A} \right]. \quad (13)$$

The molar polarizability is calculated and listed in Table 4, where the obtained values of the high-frequency dielectric constant, ε_∞ , and the lattice dielectric constant, ε_L , reveal that the electronic polarizability has primary control. The low value of dielectric constant and molar polarizability are candidates for the application of multilevel interconnections as insulators [76,80].

5 Conclusion

The XRD obtained for NiTTP powder and thin films confirms that the material is polycrystalline with monoclinic structure. Miller indices, $h k l$, values for each diffraction peak were also calculated. SEM topographs of as-deposited NiTTP films depicted that the prepared films with a nanoporous nature and its microstructure contain nanoscaled granular particles of sizes 49.7, 64.7 and 107 nm. The films' topography and porosity were increased after the annealing process at 423 K and 573 K in comparison to the prepared films at 298 K. The deduced analysis of the topographical and microstructural properties of SEM topographs before and after annealing may be useful to modify the NiTTP thin films under the influence of annealing temperature to obtain predictable changes in the optical properties of NiTTP thin films before and after annealing. The optical properties of NiTTP thin films before and after annealing have been studied in the spectral range of 200–2500 nm. The recorded absorption spectra in the UV-vis regions show two absorption bands of the NiTTP molecule, the Soret (B -band) and the Q -band. The peaks of Q and B bands are assigned of π - π^* transition between bonding and anti-bonding molecular orbitals. The annealing temperatures have an effect on the excitonic

and impurity levels, which may be due to the change in the microstructure of the film.

On the other hand, the analysis examines the change in the refractive index of the as-deposited and annealed films. The calculations of the molar extinction coefficient, $\varepsilon_{\text{molar}}$, for NiTPP thin films under the influence of annealing temperatures included a theoretical study using Gaussian distribution fitting, in order to calculate the oscillator strength, f , and electric dipole strength, q^2 , which was useful to predict the probable transitions. The optical absorption edges are described using the band transition. The allowed transitions were found to be indirect transitions. The first transition, optical gap, E_g^{onset} , or excitonic gap and the last one, E_g , is the fundamental energy gap, and between them there are one or two transitions corresponding to the trap transitions. The utilized annealing temperatures have an effect on the excitonic and impurities levels, which may be due to the change in the microstructure of the film, where the former value, E_g^{onset} , was found to decrease from 1.92 to 1.15 eV and the latter value, E_g , to decrease from 2.58 to 2.39 eV by increasing the annealing temperature from 298 to 523 K.

An interpretation of single oscillator parameters and free carrier absorption model has been described for the analysis of refractive index dispersion before and after annealing. The values of the calculated dispersion parameters such as oscillator energy, E_o , and dispersion energy, E_d , were found to increase from 1.85 to 2.6 eV and 7.7 to 10.6 eV, respectively. The third-order nonlinear optical susceptibility, $\chi^{(3)}$, and molar polarizability, α_p , are also calculated for as-deposited and annealed NiTPP thin films.

The authors would like deeply to thank Dr. E.M. El-Menyawy (Solid State Physics Department, Solid State Electronics Lab, National Research Center, Dokki, Cairo, Egypt) and Dr. A.M. Hassanien, and Dr. E.F.M. El-Zaidia (Thin Film Laboratory, Physics Department, Faculty of Education, Ain Shams University, Egypt) for their valuable discussion.

References

1. C.A. Mirkin, M.A. Ratner, *Annu. Rev. Phys. Chem.* **43**, 719 (1992)
2. A. Nakano, A. Osuka, T. Yamazaki, Y. Nishimura, S. Akimoto, I. Yamazaki, A. Itaya, M. Murakami, H. Miyasaka, *Chem. Eur. J.* **7**, 3134 (2001)
3. E.D. Sternberg, D. Dolphin, C. Brückner, *Tetrahedron* **54**, 4151 (1998)
4. F. Remacle, S. Speiser, R.D. Levine, *J. Phys. Chem. B* **105**, 5589 (2001)
5. P.G. Van Patten, A.P. Shreve, J.S. Lindsey, R.J. Donohoe, *J. Phys. Chem. B* **102**, 4209 (1998)
6. A. D'Amico, C.D. Natale, R. Paolesse, A. Macagnano, A. Mantini, *Sens. Actuators B: Chem.* **65**, 209 (2000)
7. P.K.B. Palomaki, A. Krawicz, P.H. Dinolfo, *Langmuir* **27**, 4613 (2011)
8. M. Tonezzer, A. Quaranta, G. Maggioni, S. Carturan, G. Della Mea, *Sens. Actuators B: Chem.* **122**, 620 (2007)
9. D.M. Mattox *Handbook of Physical Vapor Deposition (PVD) Processing*, 2nd edn. (Elsevier/William Andrew Publishing/Noyes, 2010), ISBN 978-0-8155-2037-5
10. M. Tonezzer, G. Maggioni, A. Quaranta, S. Carturan, G. Della Mea, *Sens. Actuators B: Chem.* **122**, 613 (2007)
11. Y.-H. Zhang, W.-J. Ruan, Z.-Y. Li, Y. Wu, J.-Y. Zheng, *Chem. Phys.* **315**, 201 (2005)
12. A. Antipas, M. Gouterman, *J. Am. Chem. Soc.* **105**, 4896 (1983)
13. P.C. Ray, J. Leszczynski, *Chem. Phys. Lett.* **399**, 162 (2004)
14. M. Ashida, H. Yanag, S. Hayashi, K. Takemoto, *Acta Crystallogr. B* **47**, 87 (1991)
15. A. Stendal, U. Beckers, S. Wilbrandt, O. Stenzel, C. Von Borczyskowski, *J. Phys. B: At. Mol. Opt. Phys.* **29**, 2589 (1996)
16. R. Czolk, *Sens. Actuators B: Chem.* **30**, 61 (1996)
17. C. Di Natale, D. Salimbeni, R. Paolesse, A. Macagnano, A. D'Amico, *Sens. Actuators B: Chem.* **65**, 220 (2000)
18. K.M. Kadish, K.M. Smith, R. Guilard (eds.), *The Porphyrin Handbook*, Applications: Past, Present and Future, vol. 6 (Academic Press, New York, 2000)
19. F.M. Qureshi, S.J. Martin, X. Long, D.D.C. Bradley, F.Z. Henari, W.J. Blau, E.C. Smith, C.H. Wang, A.K. Kar, H.L. Anderson, *Chem. Phys.* **231**, 87 (1998)
20. K. Dou, X. Sun, X. Wang, R. Parkhill, Y. Guo, E.T. Knobbe, *Solid State Commun.* **107**, 101 (1998)
21. M.R. Wasieleski, *Chem. Rev.* **92**, 435 (1992)
22. N. Kobayashi, W.A. Nevin, S. Mizunuma, H. Awaji, M. Yamaguchi, *Chem. Phys. Lett.* **205**, 51 (1993)
23. D.V.G.L.N. Rao, F.J. Aranda, D.E. Remy, J.F. Roach, *Int. J. Nonlinear Opt. Phys.* **3**, 511 (1994)
24. L. Shen, M. Ratterman, D. Klotzkinb, I. Papautskya, *Sens. Actuators B: Chem.* **155**, 430 (2011)
25. L. Scudiero, K.W. Hipps, D.E. Barlow, *J. Phys. Chem. B* **132903** (2003)
26. D. Chu, R. Jiang, *Solid State Ion.* **148**, 591 (2002)
27. W. Wu, H. Zhang, Y. Wang, S. Yu, Yu. Guo, C. Di, G. Yu, D. Zhu, Y. Liu, *Adv. Funct. Mater.* **18**, 2593 (2008)
28. S. Tolansky (ed.), *Multiple-Beam Interferometry Surface and Films*, vol. 76 (Oxford University Press, London, 1978), p. 48
29. M.M. El-Nahass, *J. Mater. Sci.* **27**, 6597 (1992)
30. M. Di Giulio, G. Micocci, R. Rella, P. Siciliano, A. Tepore, *Phys. Status Solidi A* **136**, K101 (1993)
31. R. Shirley, *The CRYSFIRE System for Automatic Powder Indexing: User's Manual* (The Lattice Press, Guildford, England, 2000)
32. J. Laugier, B. Bochu, LMGP-Suite of Programs for the Interpretation of X-ray Experiments, ENSP/Laboratoire des Matériaux et du Génie Physique, Saint-Martin-d'Hères, France, 2000
33. C.Y. Lin, L.C. Chuang, G.H. Lee, S.M. Peng, *J. Organomet. Chem.* **690**, 291 (2005)
34. Z. Xiao, B.O. Patrick, D. Dolphin, *Inorg. Chem.* **42**, 8125 (2003)

35. C.S. Chang, C.H. Chen, Y.I. Li, B.C. Liau, B.T. Ko, S. Elango, J. Chen, *Inorg. Chem.* **40**, 2905 (2001)
36. P. Bhyrappa, S.R. Wilson, K.S. Suslick, *J. Am. Chem. Soc.* **119**, 8492 (1997)
37. C. Milton, E.J. Dwornik, P.A. Estep-Barnes, R.B. Finkelman, A. Pabst, S. Balmer, *Am. Mineral.* **63**, 930 (1978)
38. M.O. Senge, M. Davis, *Acta Crystallogr. Sect. E.* **66**, 7 (2010)
39. A. Imhof, D.J. Pine, *Nature* **389**, 948 (1997)
40. J.-H. Chou, M.E. Kosal, H.S. Nalwa, N.A. Rakow, K.S. Suslick, in *The Porphyrin Handbook*, edited by K.M. Kadish, K.M. Smith, R. Guilard, vol. 4 (Academic Press, San Diego, CA, USA, 2000), pp. 43–131
41. O. Stenzel, S. Wilbrant, A. Stendal, U. Beckers, K. Voigtsberger, C. Von Borczkowski, *J. Phys. D* **28**, 2154 (1995)
42. S.H. Wemple, M. DiDomenico, *Phys. Rev. B* **3**, 1338 (1971)
43. S.H. Wemple, *Phys. Rev. B* **7**, 3767 (1973)
44. M.M. El-Nahass, A.F. El-Deeb, H.S. Metwally, A.M. Hassanien, *Mater. Chem. Phys.* **125**, 247 (2011)
45. D.V. Konarev, A.Y. Kovalevsky, X. Li, I.S. Neretin, A.L. Litvinov, N.V. Drichko, Y.L. Slovokhotov, P. Coppens, R.N. Lyubovskaya, *Inorg. Chem.* **41**, 3638 (2002)
46. A.S. Davydov, *Theory of Molecular Excitons* (Plenum Press, New York, 1971)
47. W.R. Scheidt, Y.J. Lee, *Struct. Bondin (Berlin)* **1**, 64 (1987)
48. M.M. El-Nahass, A.H. Ammar, A.A.M. Farag, A.A. Atta, E.F.M. El-Zaidia, *Solid State Sci.* **13**, 596 (2011)
49. E.J. Baerends, G. Ricciard, A. Rosa, S.J. Van Gisbergen, *Coord. Chem. Rev.* **230**, 5 (2002)
50. M.M. El-Nahass, H.M. Zeyada, M.S. Aziz, M.M. Makhlof, *Spectrochim. Acta Part A* **62**, 11 (2005)
51. G. Scott, L.A. Harry, *Chem. Commun.* 1539 (1999)
52. G.A. Kumar, G. Jose, V. Thomas, N.V. Unikrishnan, V.P.N. Nampoore, *Spectrochim. Acta A* **59**, 1 (2003)
53. G. Kumar, J. Thomas, N. George, B. Kumar, P. Radhakrishnam, *Phys. Chem. Glass* **41**, 199 (2000)
54. U. Pal, D. Samanta, S. Ghori, A.K. Chaudhuri, *J. Appl. Phys.* **74**, 6368 (1993)
55. E.V. Tsiper, Z.G. Soos, W. Gao, A. Kahn, *Chem. Phys. Lett.* **360**, 47 (2002)
56. U. Zhokhavets, R. Goldhahn, G. Gobsch, W. Schliecke, *Synth. Met.* **138**, 491 (2003)
57. G. Li, V. Shrotriya, Y. Yao, Y. Yanga, *J. Appl. Phys.* **98**, 043704 (2005)
58. M. Ghanashyam Krishna, J.S. Pillier, A.K. Bhattacharya, *Thin Solid Films* **357**, 218 (1999)
59. P.O. Edward, *Handbook of Optical Constants of Solids* (Academic Press, New York, 1985), p. 265
60. J.B. Yadav, R.K. Puri, V. Puri, *Appl. Surf. Sci.* **253**, 8474 (2007)
61. T. Rechardson, K. von Rottkay, J. Slack, F. Michalak, M. Rubin, Ernest Orlando Lawrence Berkeley National Laboratory, Berkeley, USA
62. M. Zhu, L. Liu, Y. Hou, H. Yan, J.B. Xu, M. Shao, X. Chen, *Physica B* **355**, 100 (2005)
63. R.C. Miller, *Appl. Phys. Lett.* **5**, 17 (1964)
64. C.C. Wang, *Phys. Rev. B* **2**, 2045 (1970)
65. L. Tichy, H. Ticha, P. Nagels, R. Callaerts, R. Mertens, M. Vlcek, *Mater. Lett.* **39**, 122 (1999)
66. M.C. Gupta, *Handbook of Photonics* (CRC Press, Boca Raton, FL, 1997)
67. M. Gamboa, M. Campos, L.A. Torres, *J. Chem. Thermodyn.* **42**, 666 (2010)
68. A. Wahab, M. Bhattacharya, S. Ghosh, A.G. Samuelson, P.K. Das, *J. Phys. Chem. B* **112**, 2842 (2008)
69. U. Zhokhavets, R. Goldhahn, G. Gobsch, W. Schliecke, *Synth. Met.* **143**, 113 (2004)
70. K. Maex, M. Baklanov, M. Green (eds.), *Dielectric Films for Advanced Microelectronics*, Materials for Electronic and Optoelectronic Applications Series (John Wiley & Sons, Ltd., New York, 2007), p. 299
71. S.P. Murarka, M. Eizenberg, A.K. Sinha (eds.), *Inter-layer Dielectrics for Semiconductor Technologies, Technology and Engineering* (Academic Press, London: Elsevier, 2003), pp. 7–36
72. V. Ksianzou, R.K. Velagapudi, B. Grimm, S. Schrader, *J. Appl. Phys.* **100**, 63106 (2006)
73. G.D. Mahan, K.R. Subbaswamy, *Local Density Theory of Polarizability* (Plenum Press, New York, 1990)
74. O.S. Heavens, *Optical Properties of Thin Solid Films* (Dover Publications, New York, 1965)
75. H. Fröhlich (ed.), *Theory of Dielectrics*, 2nd edn. (Clarendon Press, Oxford, 1958)
76. J.H. Choi, Ch.S. Korach, *J. Electrochem. Soc.* **12**, 961 (2009)
77. K. Kobayashi, *J. Phys. Chem. Solids* **59**, 1671 (1998)
78. M. Bala Murali Krishna, V. Praveen Kumar, N. Venkatramaiah, R. Venkatesan, D. Narayana Rao, *Appl. Phys. Lett.* **98**, 081106 (2011)
79. S.A. Krasnikov, N.N. Sergeeva, M.M. Brzhezinskaya, A.B. Preobrajenski, Y.N. Sergeeva, N.A. Vinogradov, A.A. Cafolla, M.O. Senge, A.S. Vinogradov, *J. Phys.: Condens. Matter* **20**, 235207 (2008)
80. F.J. Pavinatto, A.F. Gameiro Jr., A.A. Hidalgo, L.R. Dinellid, L.L. Romualdoe, A.A. Batistae, N.M. Barbosa Netoc, M. Ferreirab, O.N. Oliveira Jr., *Appl. Surf. Sci.* **254**, 5946 (2008)